Compact Leaky Wave Fed Frequency-Scanning Gradient Index Lens Antenna for Near-Field-Focusing Applications

Kevin Kipruto Mutai, *Graduate Student Member, IEEE*, and Qiang Chen, *Senior Member, IEEE*

***Abstract*— In this article, a compact antenna structure capable of focusing in the near field and composed of a gradient index (GRIN) lens and a frequency-scanning, longitudinally slitted waveguide feed is proposed. The slitted waveguide can support traveling waves propagating with both a positive and negative phase constant (β), thereby allowing scanning between the backward and forward quadrants. The scanning is realized by varying the frequency from 26 to 35 GHz achieving a total displacement of the focusing spot of about 125 mm along the *z*-direction in the H-plane.**

***Index Terms*— 3-D printing, additive manufacturing (AM), frequency-scanning antennas (FSAs), gradient index (GRIN) lens antenna, leaky wave antennas (LWAs), Mikaelian lens, near-field focusing (NFF), slot arrays.**

I. Introduction

OWING to their inherent characteristic to scan along one end by changing the position of the feed located at the opposite end plane [1], gradient index (GRIN) lens-based antennas have attracted significant interest as beamforming solutions [2]. Furthermore, these structures are often of a wideband nature and are flexibly able to meet requirements for various application areas [3], [4] with the only limitation being the dispersion of the dielectric material used to fabricate the lens. One such area of interest is applications requiring near-field focusing (NFF) [5], [6], where the focusing effect can be achieved by appropriately tapering the GRIN lens profile.

A class of GRIN lenses that is particularly attractive is the Mikaelian lens, given its planar and therefore small and easily integrable, physical profile [1], [7], [8], [9]. Beam scanning using the Mikaelian lens was explored in [10], where an open-ended waveguide was mechanically scanned across the aperture of the lens, and in [11], where an array of patch antennas was used to feed the lens and scanning was electronically achieved by appropriately turning on and off the antennas. To further simplify the scanning along one dimension and avoid the bulky, time-consuming mechanical approach or the complicated multiport approach, we propose to use a slitted waveguide capable of both a positive and negative β, thereby theoretically allowing scanning through the broadside from the backward quadrant to the forward quadrant of the region above the combined structure composed of the Mikaelian lens and slitted waveguide feed (see Fig. 1).

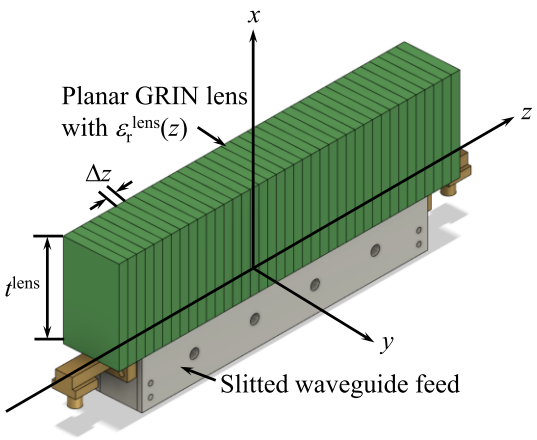

Fig. 1. Proposed leaky wave-fed planar GRIN lens antenna.

The novelty in the proposed approach lies in exploiting both the frequency-scanning capability of the slitted waveguide feed to instantaneously scan along the H-plane (the *xz*-plane in this work as viewed from within the waveguide for convenience) and the ease with which the focusing effect can be achieved by tapering the profile of the Mikaelian lens by 3-D printing. leaky wave antennas (LWAs) capable of NFF have been studied extensively [12], [13], [14], [15], [16], [17], [18], [19], [20], [21], [22], [23], [24], [25], [26], [27], [28], [29], [30], where both the feed and phase tapering mechanisms are combined in a single structure, which, though providing a more compact form factor, necessitates complicated designs, thereby increasing the fabrication complexity as the antenna structures require specific mechanical modifications to taper the traveling wave in some manner. Moreover, as a consequence of these mechanical modifications, the various antennae's focusing characteristics cannot be flexibly changed should the application needs change which would mean the refabrication of the entire antennae's structures which might be a relatively time consuming and expensive endeavor.

Manuscript received 6 August 2023; revised 29 November 2023; accepted 9 January 2024. Date of publication 19 January 2024; date of current version 7 March 2024. This work was supported in part by the Program on Open Innovation Platform with Enterprises, Research Institute and Academia, Japan Science and Technology Agency (OPERA, JST) under Grant JPMJOP1852. *(Corresponding author: Kevin Kipruto Mutai.)*

The authors are with the Department of Communications Engineering, Graduate School of Engineering, Tohoku University, Sendai, Miyagi 980-8579, Japan (e-mail: mutai-k@ecei.tohoku.ac.jp; chenq@ecei.tohoku.ac.jp).

Color versions of one or more figures in this article are available at https://doi.org/10.1109/TAP.2024.3353375.

Digital Object Identifier 10.1109/TAP.2024.3353375

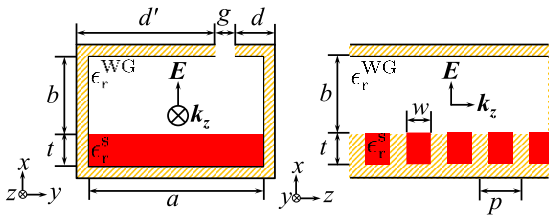

Fig. 2. Slitted waveguide feed structure viewed from (a) transverse direction and (b) longitudinal section.

To alleviate these issues, the feed is separated from the phase tapering in this work, which affords us an extra degree of freedom in the proposed design relative to the conventional tapered LWAs. As such, in the proposed work, it is theoretically possible to change the focusing characteristics of the combined structure simply by switching out the cheaply and rapidly 3-D printed GRIN lens superstrate depending on the application scenario. Additionally, having an untapered LWA as a feed reduces the fabrication complexity as mechanical modification of the guiding structure is unnecessary. The design of the slitted waveguide feed and the GRIN lens is treated in Section II. Experimental results to verify the focusing effect are presented and discussed in Section III.

II. Design of the Slitted Waveguide Feed and GRIN Lens Sections

A. Slitted Waveguide Feed

The waveguide feed to the GRIN lens is based on the corrugated waveguide with dielectric fillings proposed in [31] that is capable of supporting traveling waves with a positive and negative β. By using dielectric material in the corrugations, an electric field is induced within the corrugation with a vector that lies along the longitudinal direction of the waveguide region (z-direction) that is in the cutoff region of the dominant mode of operation of the waveguide region. The corrugations therefore act as periodic scatterers deflecting this induced field backward generating the $-\beta$ traveling waves within the air-filled waveguide region above the corrugations. When the frequency is increased, the dominant mode of the waveguide region appears, and the traveling wave then proceeds to the positive z-direction with a positive β as normal.

To design the $\pm\beta$ waveguide, the physical model shown in Fig. 2 was used. Taking the reference plane at $x = t$ for a single corrugation in the model, the bottom region containing the periodic dielectric-filled corrugation and the air-filled waveguide region above can be viewed as short circuits. The model can therefore be described in circuit network terms by the following set of equations and resolved by the transverse resonance method [32] with $g = 0$. First, the bottom and upward admittances viewed from $x = t$ are described as

$$Y_{\text{tot}} = Y_0 + Y_1 = 0 \tag{1}$$

where Y_0 is the input admittance of the corrugation and Y_1 is that of the waveguide region. These two values are expressed by

$$Y_0 = \frac{k_{x0}}{\omega\mu_0}\left[\frac{wa}{2p}\frac{\gamma^2}{k_{x0}}\left(\frac{\sin\left(k_z\frac{w}{2}\right)}{k_z\frac{w}{2}}\right)^2\right] j\cot(k_{x0}b) \tag{2}$$

$$Y_1 = \frac{k_{x1}}{\omega\mu_0}\cot(k_{x1}t) \tag{3}$$

for the fundamental, dominant TE mode of the waveguide with the periodicity of the corrugation being catered to by the term in square brackets in (2). The specific terms in (2) and (3) are given as

$$k_{x0} = \sqrt{\epsilon_{\text{r}}^{\text{WG}}k_0^2 - \left(k_z^2 + \left(\frac{\pi}{a}\right)^2\right)} \tag{4}$$

$$\gamma = \sqrt{\epsilon_{\text{r}}^{\text{WG}}k_0^2 - \left(\frac{\pi}{a}\right)^2} \tag{5}$$

$$k_{x1} = \sqrt{\epsilon_{\text{r}}^{\text{s}}k_0^2 - \left(\frac{\pi}{a}\right)^2}. \tag{6}$$

To resolve for k_z, (2)–(6) can be substituted into (1) and solved numerically within solution limits of interest with the imaginary part (corresponding to the attenuation constant α) set as zero as no radiation occurs. The real part of the solutions is then the β and the results for the closed waveguide ($g = 0$) in the frequency range of 25–35 GHz are indicated by the black line in Fig. 3 as calculated by the circuit model. The parameters used were selected to allow a smooth transition between the $-\beta$ and $+\beta$ regions within the desired frequency range of operation, and as we are primarily interested in the leaky waves ($\beta < k_0$) capable of radiating, the solution limits were set with $|\beta| < k_0$, which explains why we describe the proposed structure as leaky wave fed. The circuit model with $g = 0$ can be used to rapidly determine the optimal physical parameters of the waveguide feed before introduction of the slit to enable radiation.

To allow the radiation of the traveling wave, a thin longitudinal slit is introduced at an offset along the broad wall of the waveguide. This is because along the center, the surface current density distribution along the internal walls of the waveguide is nulled at the dominant mode, and if a thin slit is cut along this region, there would be no radiation. Of course, this can be resolved by increasing the slit width; however, there would be symmetrically opposed magnetic current vectors within the longitudinal slit, which then cancel out and the problem remains. As a solution to this issue, the slit position can be offset, causing an asymmetry thereby allowing radiation from the waveguide [33].

The k_z characteristics of the slitted waveguide model were extracted by full-wave simulation software and compared with the slitted waveguide results ($g = 1$ mm) in Fig. 3(a). From these results, it appears that the addition of a thin longitudinal slit has a noticeable effect on β. Specifically, the red line corresponding to the $g = 1$ mm case can be seen to flatten, which suggests that the radiation direction would be closer to the broadside in both the lower and higher frequency regions, which would imply a reduced total scanning range. The red line can also be seen to jump from a value of

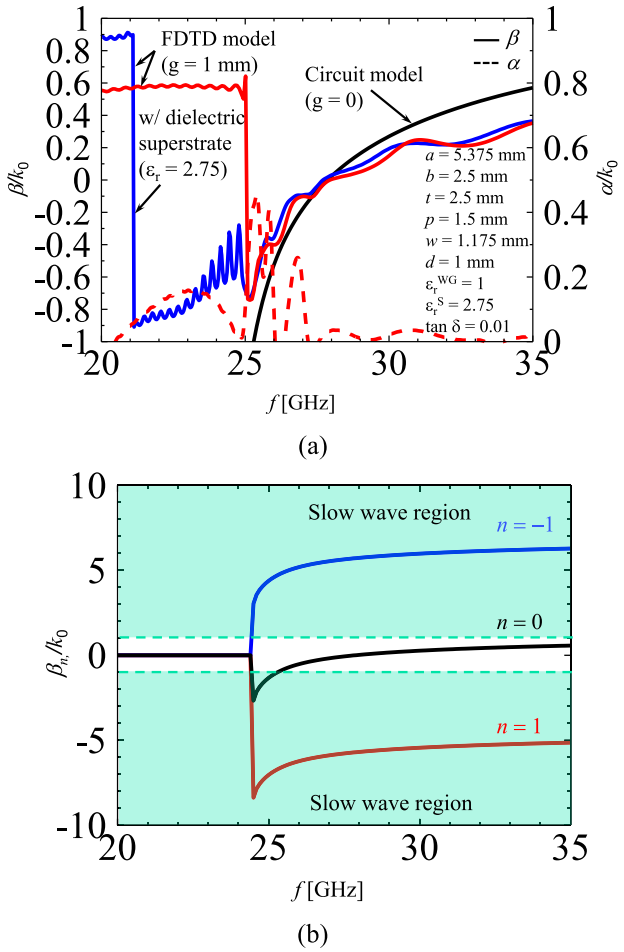

Fig. 3. (a) Normalized propagation constant of the slitted waveguide feed ($n = 0$ space harmonic) obtained from full-wave simulation (FDTD) and the circuit model and (b) normalized phase constants of the $n = -1$, $n = 0$, and $n = 1$ space harmonics extracted from the circuit model.

about -0.74 at around 25 GHz to about 0.6 at frequencies lower than 25 GHz. This phenomenon, and the relatively constant value of β between 20 and 25 GHz, may be attributed to the slot mode that appears between the parallel edges of the longitudinal slit [34] even in the cutoff region of the waveguide below the slit and can be suppressed from radiating by using shorter transverse slots [35] as is done in this work. Although the slot mode can be suppressed from radiating by using the shorter transverse slots, its propagation within the waveguide proceeds unimpeded, which leads to the extraction of both the slot mode and the fundamental TE mode from the full-wave simulation (FDTD) model, which explains the ripples appearing in the red and blue β curves for frequencies larger than 25 GHz.

There is an increase in α in the $-\beta$ region, which may be because the slitted waveguide is operating in the cutoff region of the normal operating mode of the waveguide. This increase in α means that the effective radiating length of the slitted waveguide would be reduced in the $-\beta$ region compared to the $+\beta$ region, which would lead to a reduced magnitude of the electric field in this region. This phenomenon might be solved by tapering of α in taking this variation into account and is to be further studied in future iterations of the structure proposed here. There is also a drop in α as the frequency is increased from 27 GHz, which is caused by the slitted waveguide approaching an open stopband (OSB), which suggests that no radiation would take place at this frequency, and consequently, a dip in the magnitude of the radiated electric field is expected. At and below the cutoff frequency, α assumes a finite value, which is a phenomenon associated with the previously discussed slot mode.

If the slit along the top of the slitted waveguide was composed of only the longitudinal slit, the main vector of the radiated electric field would be along the y-direction. However, because shorter transverse slots are introduced periodically along the slit to suppress the radiation of the slot mode, the linear polarization of the radiated field is also shifted by 45° from the y-axis.

To confirm the influence of adding the GRIN lens on top of the slitted waveguide on the β, a model of the slitted waveguide with a dielectric slab ($\varepsilon_r = 2.75$ and $\tan\delta = 0.01$) positioned on top of the waveguide was calculated and the β extracted and plotted as the blue line in Fig. 3(a). From the figure, we may infer that the addition of a dielectric superstrate has the effect of somewhat suppressing the slot mode from propagating in the frequency range 21–25 GHz though not completely as indicated by the presence of ripples in the curve. It also appears that the addition of the lens would have minimal influence on the TE mode propagating within the waveguide as there is a small difference between the red and blue lines from 25 GHz and above.

As the corrugated waveguide is periodic in nature, the k_z values of the $n = -1$ and $n = 1$ space harmonics were calculated in addition to those of the fundamental $n = 0$ harmonic using the expression

$$k_{zn} = k_{z0} + \frac{2n\pi}{p} \tag{7}$$

where k_{z0} is the k_z of the $n = 0$ space harmonic and p is the periodicity of the corrugations and the results presented in Fig. 3(b). Since a common value of α is shared among the various space harmonics [36], only β is included in Fig. 3(b) and α in Fig. 3(a) should suffice for the analysis of the attenuation characteristics. As the slitted waveguide primarily exploits the $n = 0$ space harmonic to accomplish scanning from the backward quadrant to the forward quadrant, it follows that the $n = -1$ and $n = 1$ space harmonics should be confined within the waveguide ($|\beta_n/k_0| > 1$) as slow waves to ensure there is no interference with the radiated field once a slit is introduced and this appears to be the case in the proposed structure as observed from the figure.

The length of the feed to the lens was set as $L = 103.5$ mm both for manufacturing convenience and easy periodicity of the corrugations introduced into the bottom surface of the slitted waveguide feed. With this value in mind, the next step was to determine the optimal α/k_0 that would ensure a radiation efficiency, $\eta_{\text{rad}} = 0.9$ at the desired center frequency of 28 GHz (decided upon from the frequency characteristics of β presented in Fig. 3), which was obtained from

$$\eta_{\text{rad}} = 1 - e^{-2\int_{-0.5L}^{0.5L}\alpha(z')dz'} \tag{8}$$

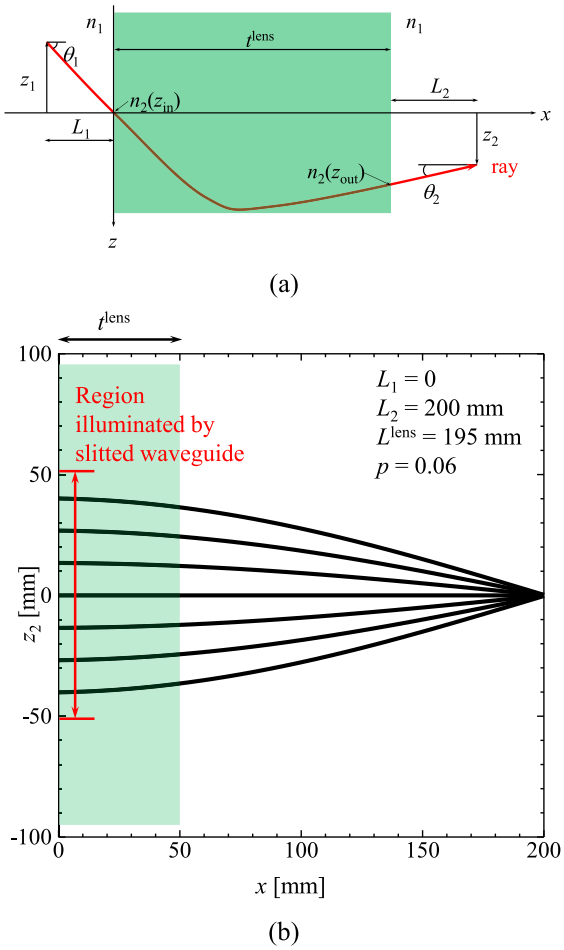

Fig. 4. Ray trajectory through (a) nongeneralized Mikaelian lens and (b) with $t^{\text{lens}} = 50$ mm, $L_1 = 0$, $L_2 = 200$ mm, and $p = 0.06$ in the case of a leaky wave feed.

as $\alpha/k_0 = 0.02$ and the slit width $g = 1$ mm was found to ensure this leakage rate at 28 GHz by full-wave simulations.

B. Planar (Mikaelian) GRIN Lens

To gain physical insight into the self-focusing property of the Mikaelian lens, the ray tracing model shown in Fig. 4(a) was used. In the model, z_1 indicates the position of the source along the z-direction of the ray feeding the lens at L_1 from the lens surface. The thickness of the lens is given by t^{lens} and z_2 is the position of the ray at the output of the lens at L_2 from the lens surface. The generalized ray trajectory through the lens can then be determined by using the following matrix [37], [38]:

$$\begin{bmatrix} z_2 \\ \theta_2 \end{bmatrix} = \begin{bmatrix} 1 & L_2 \\ 0 & 1 \end{bmatrix} \begin{bmatrix} 1 & 0 \\ 0 & \frac{n_2(z_{\text{in}})}{n_1} \end{bmatrix} \begin{bmatrix} \cos gz & \frac{1}{n_1 g}\sin gz \\ -n_1 g \sin gz & \cos gz \end{bmatrix} \cdot \begin{bmatrix} 1 & 0 \\ 0 & \frac{n_1}{n_2(z_{\text{out}})} \end{bmatrix} \begin{bmatrix} 1 & L_1 \\ 0 & 1 \end{bmatrix} \begin{bmatrix} z_1 \\ \theta_1 \end{bmatrix} \quad (9)$$

where $g = 2\pi p/t^{\text{lens}}$, in which p is the pitch, $n_2(z_{\text{in}})$ and $n_2(z_{\text{out}})$ are the refractive indices at the points of incidence and output, respectively, and n_1 is the refractive index of air.

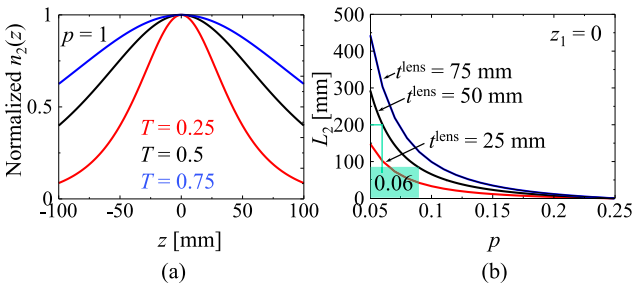

Fig. 5. (a) Refractive index profiles of the Mikaelian lens with different values of T with $D = 200$ mm. (b) Focal length L_2 of the Mikaelian lens with changing values of t^{lens} and p.

The refractive index profile of the Mikaelian lens is given as [1]

$$n_2(z) = \frac{n_2(0)}{\cosh \frac{2\pi p z}{t^{\text{lens}}}}. \quad (10)$$

The relationship between the refractive index profile and the thickness of the lens was then investigated and the results indicated in Fig. 5(a) where $T = t^{\text{lens}}/L^{\text{lens}}$, in which L^{lens} is the length of the lens. Increasing the thickness has the effect of flattening the refractive index profile, which would allow for more practically realizable GRIN profiles though at the cost of an increased physical profile.

Owing to the self-focusing properties of the GRIN lens, the ray trajectory through the lens can be controlled by judiciously selecting the value of pitch, p, to achieve a desired focusing performance. As the lens will be fed by the line source presented by the slitted waveguide, which will be presented as a plane wave at the interface with the lens, p needs to be selected, such that the aperture of the lens will be illuminated by a plane wave and the incident field be tuned to focus on some desired L_2 in the Fresnel region. The influence of p on L_2 was then studied using the following expression [39]:

$$L_2 = \frac{t^{\text{lens}}}{2\pi p n_1} \cot(2\pi p) \quad (11)$$

and the results for different t^{lens} values given in Fig. 5(b). To satisfy the requirement for plane wave illumination and $L_2 = 200$ mm in the Fresnel region with a practically realizable $n_2(z)$, the pitch was set as $p = 0.06$ and $t^{\text{lens}} = 50$ mm. The value of $L^{\text{lens}} = 195$ mm was selected because we primarily wish to avoid a situation, where the left and right sides as well as the upper corners of the lens are illuminated (especially at lower and higher frequencies) by the longitudinal slit, which would lead to unwanted diffraction that would deteriorate the performance of the structure. The extra length of the lens also allows the slitted waveguide to be firmly affixed to the lens for mechanical stability.

The focusing performance of the proposed structure can then be predicted from (9) after plugging in (10), which has been calculated with $L^{\text{lens}} = 195$ mm, $t^{\text{lens}} = 50$ mm, and $p = 0.06$. The results of the ray trajectory through and out of the lens with these parameters are provided in Fig. 4(b), where the focusing position is found to be at $x = 200$ mm as opposed to the expected $x = 250$ mm ($L_2 + t^{\text{lens}}$). This is because even through $L^{\text{lens}} = 195$ mm, the actual illuminated

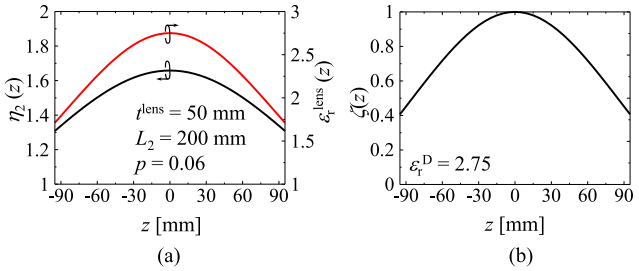

Fig. 6. (a) Refractive index profiles of the Mikaelian lens and (b) its equivalent infill ratio profile.

length of the lens is equal to $L = 103.5$ mm giving rise to the observed phenomenon.

Having settled upon the design parameters of the Mikaelian lens, the next step was to then actualize the required refractive index profile $[n_2(z)]$. To accomplish this, 3-D printing by fused deposition modeling (FDM) was settled upon as the most convenient, low-cost method. The GRIN profile would be fabricated by using an infill ratio profile $[\zeta(z)]$ that would allow the tapering of the effective relative permittivity $[\varepsilon_r^{lens}(z)]$, and therefore the refractive index, of the lens [40].

The $n_2(z)$ and subsequent $\varepsilon_r^{lens}(z)$, of the Mikaelian lens with the decided upon design parameters were calculated and are shown in Fig. 6(a). The relationship between $\varepsilon_r^{lens}(z)$ and $\zeta(z)$ is given as

$$\zeta(z) = \frac{\epsilon_r^{lens}(z) - 1}{\epsilon_r^D - 1} \tag{12}$$

where ε_r^D is the dielectric constant of the 3-D printer material. Therefore, using (12), the GRIN profile was fabricated by varying the infill ratio of the 3-D printer material at intervals of $\Delta z = 5$ mm, which was decided upon to maximize the accuracy of the commercial FDM 3-D printer to be used. The 3-D printer material used in this work to fabricate both the lens and the dielectric fillings of the corrugated waveguide is polylactic acid (PLA), which has the dielectric constant $\varepsilon_r^D \approx 2.75$ and loss tangent $\tan\delta \approx 0.01$.

Before fabrication of the slitted waveguide feed and 3-D printed Mikaelian lens prototypes, the focusing performance was confirmed by full-wave simulation, where these structures were modeled with the finalized design parameters. First, the 2-D electric field distribution in the H-plane (xz-plane) was extracted and is shown in Fig. 7(a), where the focusing position in the broadside case (28 GHz) can be seen to coincide with the predicted $x = 200$ mm in Fig. 4(b). To observe the anticipated shift in the focused spot with frequency, the 2-D electric field distribution at 26 and 35 GHz (the minimum and maximum scanning frequencies) is presented in Fig. 7(b) and (c). From these figures, the focusing spot is displaced along the x-direction as the frequency is shifted away from the design frequency with the observed displacement being about 45 mm lower than at the designed focusing position at $x = 200$ mm. This displacement is a shortcoming of the proposed structure and can be mitigated by following a conformal approach as was done in [27]. In Fig. 7(b), a weaker component of the radiated field may be observed in the backward quadrant, which is associated with

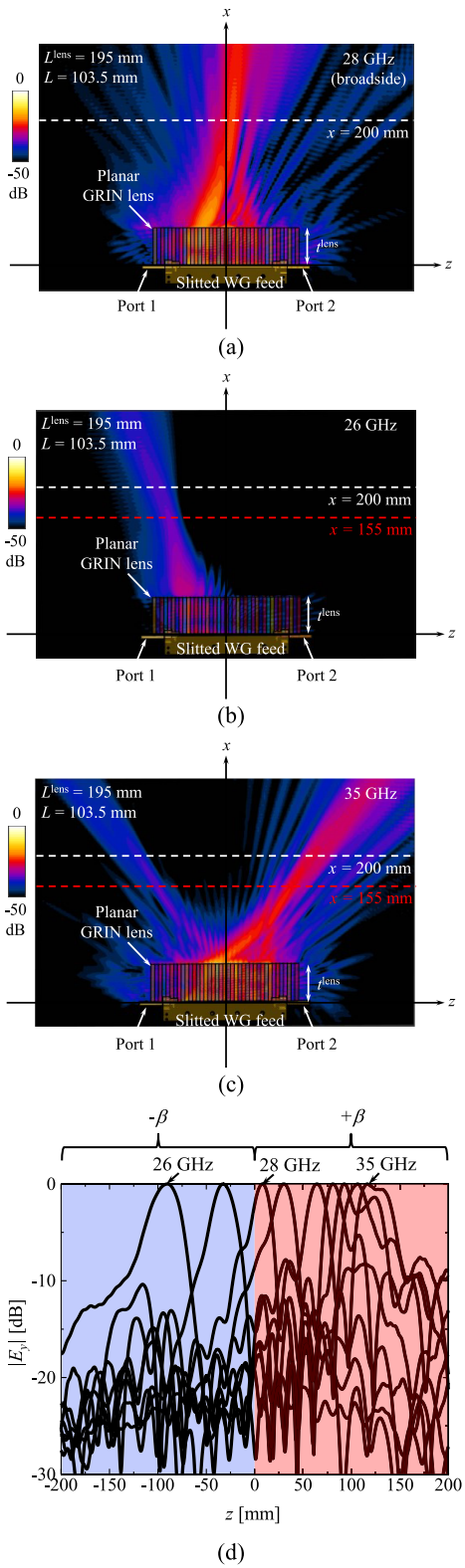

Fig. 7. (a) Simulated 2-D electric field distribution in the broadside case (28 GHz). (b) Minimum scanning frequency of 26 GHz. (c) Maximum scanning frequency of 35 GHz. (d) Normalized electric field distribution along the z-direction extracted from the simulation results at $x = 200$ mm for 26–35 GHz in 1-GHz intervals.

the next higher mode of the corrugated waveguide appearing as the frequency is increased. This mode may be suppressed by appropriate selection of the physical parameters of the

waveguide and, depending on the application scenario, would potentially have the effect of somewhat limiting the available scanning range should it be allowed to radiate.

From Fig. 7(b), the electric field generated in the backward zone ($-\beta$ region) appears to be lower than in the broadside and forward zone ($+\beta$ region) cases and this is because of the α increase observed in this region from Fig. 3(b). The normalized 1-D electric field distribution along the z-direction was extracted for different frequencies and is shown in Fig. 7(d). From the figure, the shift in the focused spot with frequency is evident ($z_{\min} = -91$ mm and $z_{\max} = 124$ mm), and when the frequency is increased, the full-width at half-maximum (FWHM) increases, which is brought about by the displacement of the focusing spot along the x-direction as the frequency is shifted away from the design frequency.

The minimum FWHM of about 20.1 mm was observed close to the broadside as expected as this position coincides with the boresight of the antenna with the given setup (antenna is fixed with the center at $z = 0$). Although the FWHM increases at the lower and higher frequencies, we believe that the increase in value is not so high as to discredit the usefulness of the proposed structure as an NFF antenna in most practical applications requiring a fixed FWHM value along the z-direction. The faster shift in the radiation direction in the backward zone compared with the forward zone when the frequency is increased is due to the steeper gradient of β in the negative region compared to the positive region, as indicated in Fig. 3. With these results validating the proposed structure's focusing and frequency-scanning capabilities, the slitted waveguide feed and planar Mikaelian lens prototypes were then fabricated and are shown in Fig. 8.

III. Experiment and Discussion

The combined prototype was measured using an experimental setup designed to replicate the full-wave simulation setup. The experiment setup is shown in Fig. 9, where the *Ka*-band open-ended waveguide (OEWG) was used as a probe and was scanned along the z-direction in the range -150 mm $\leq z \leq$ 150 mm at $x = 200$ mm and the transmission co-efficient between the leaky wave-fed lens antenna and the OEWG probe (S_{21}) was extracted at each position of the OEWG. The OEWG holder was 3-D printed to have an effective relative permittivity $\varepsilon_r^h \approx 1.44$ to minimize reflections to the device under test. Absorber material was positioned around the OEWG probe and on the floor upon which a foam platform was used to support the device under test.

To evaluate the performance of the leaky wave-fed GRIN lens antenna, both ports of the structure were connected to an ANRITSU MS46322B vector network analyzer (VNA) with and without the lens part attached and both the reflection coefficient (S_{11}) and the S_{21} measured with the results shown in Fig. 10(a).

From the figure, the addition of the lens structure to the slitted waveguide feed has minimal influence on $|S_{11}|$, which suggests minimal reflection from the lens surface back to feed port when $L_1 = 0$. Interestingly, upon addition of the lens, $|S_{21}|$ decreases, and this may be attributed to the increase in α when the lens is positioned above the slitted waveguide.

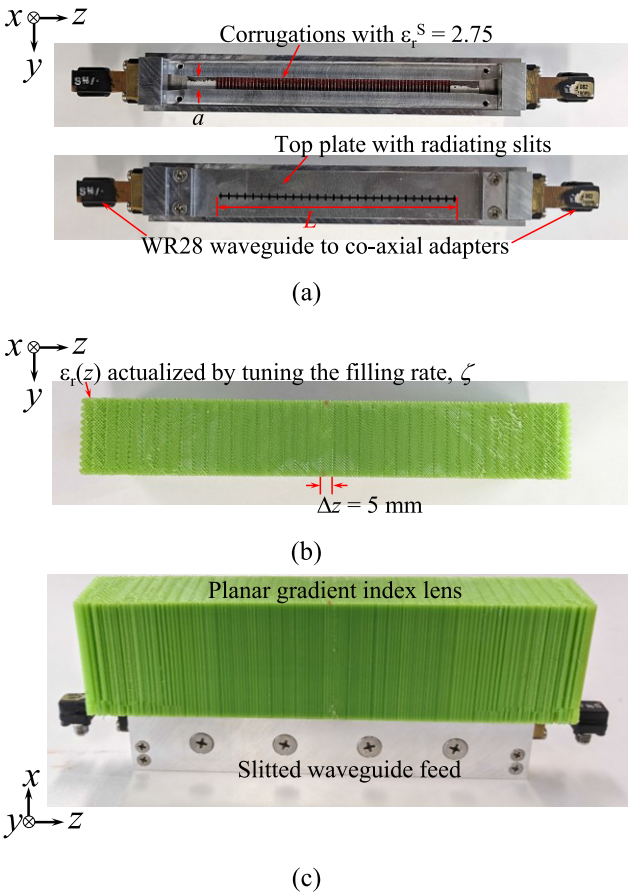

Fig. 8. (a) Fabricated slitted waveguide feed without and with the top radiating plate attached. (b) Three-dimensional printed planar Mikaelian lens with a varying infill ratio and $\Delta z = 5$ mm. (c) Combined Mikaelian lens with attached slitted waveguide feed.

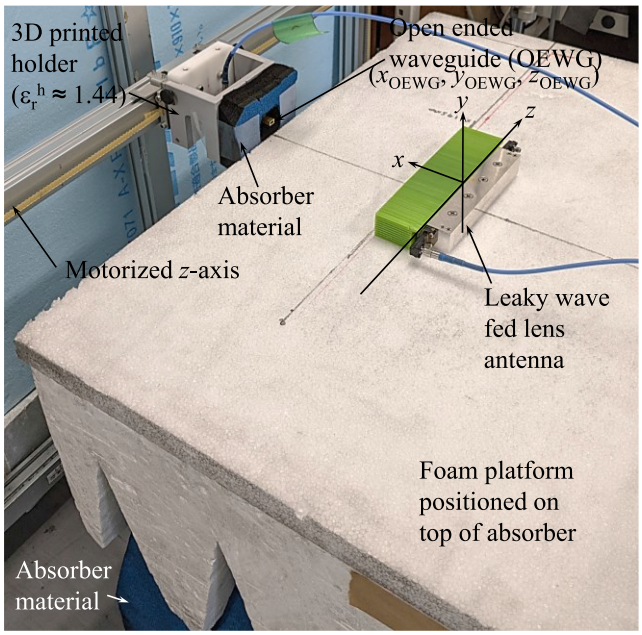

Fig. 9. Experimental setup used to measure the proposed antenna structure.

The spillover efficiency of both cases was then calculated by the equation

$$\eta_s = 1 - |S_{11}|^2 - |S_{21}|^2 \tag{13}$$

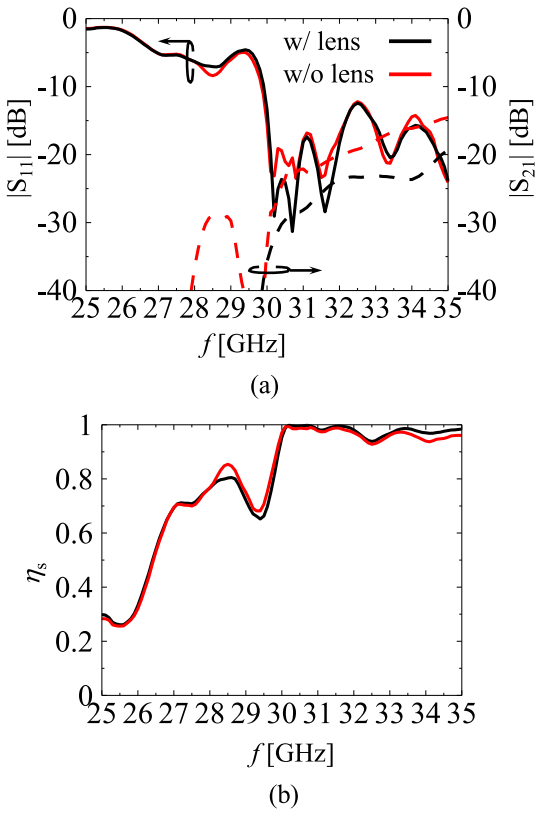

Fig. 10. (a) Measured reflection (S_{11}) at port 1 and transmission between ports 1 and 2 (S_{21}) of the leaky wave-fed GRIN lens antenna with and without the lens. (b) Measured spillover efficiency, η_s, of the antenna structure with and without the lens.

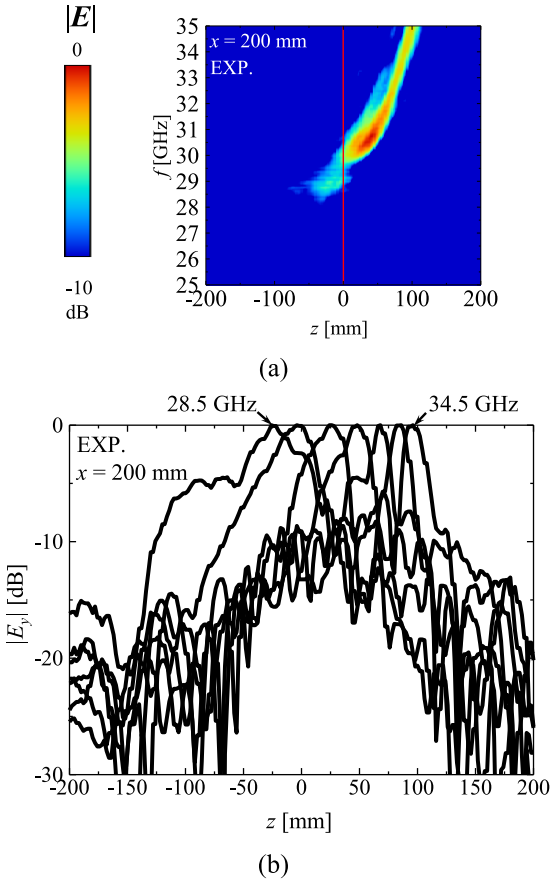

Fig. 11. (a) Measured transmission coefficient between the OEWG (oriented at 45° from the y-axis) and the leaky wave-fed GRIN antenna. (b) Normalized electric field distribution along the z-direction extracted from the measurement results at $x = 200$ mm for 28.5–34.5 GHz in 1-GHz intervals.

and the results indicated in Fig. 10(b). As the power dissipated within the waveguide by the lossy dielectric fillings is not considered in (12), it is anticipated that η_{rad} would be lower than η_s should this dissipation be considered [41]. From the results, both cases with and without the lens have similar performance in terms of η_s. η_s in the case without the lens at the center frequency 28 GHz was found to be 0.85, which is close to the designed $\eta_{rad} = 0.9$. The low η_s in both cases in the low-frequency region is due to the dominant mode being in the cutoff region, and as such, the amount of radiated power is anticipated to be low. The dip observed at about 29.5 GHz is theorized to be because of the fabricated slitted waveguide approaching the OSB close to broadside.

To evaluate the focusing effect at $L_2 = 200$ mm, the extracted electric field distribution for different frequencies was plotted in Fig. 11. From the simulation results in Fig. 7(b), it appears that the focusing effect at $z = 0$ mm was achieved close to 28 GHz, whereas in the measurement results, it was observed close to 29.5 GHz. Additionally, it appears that the achieved measured scanning range of the proposed structure is from $z_{min} = -26$ mm to $z_{max} = 98$ mm at $x = 200$ mm, giving a total displacement along the z-direction of 124 mm, which is lower than the 215 mm observed from the simulation results in Section II-B and Fig. 7(b). The FWHM of the measured frequency-scanned focused spot varies from about 40 mm at 28.5 GHz to about 20 mm at 34.5 GHz, which is different to the theoretically predicted results. These phenomena indicate a deterioration in the measured results compared to the simulation results and especially in the low-frequency operating region (concerned with $-\beta$, and therefore very sensitive to fabrication defects in the corrugations) and may be caused by the rough upper and lower surfaces of the 3-D printed dielectric fillings used in the corrugations, which distort the field within the waveguide and therefore also the radiated field. This issue can be resolved by using a 3-D printer with a finer minimum spatial resolution in addition to lower loss printer material and is to be investigated in future work. The focusing spot displacement along the x-direction and the increase in α in the backward zone are also some areas that can be further optimized upon in the next iterations of the structure proposed herein. Finally, the form factor of the proposed structure can also be made more compact should the feed design be changed to thinner waveguide structures, such as substrate integrated waveguide (SIW) technologies. Despite these difficulties, the concept of a frequency-scanning leaky wave-fed GRIN lens antenna has been successfully demonstrated.

The proposed structure was compared with other LWA-based NFF solutions on the basis of the scanning range, the complexity involved in tapering β (essentially the design flexibility), the frequency of operation, and the compactness of the structure, and the results are summarized in Table I. In the analysis of the compactness, the overall physical profile of the structures was taken into account relative to the frequency

TABLE I
COMPARISON OF NFF LWAS

Ref.	Total focusing spot displacement/ Length of antenna (z_{range}/L)	β tapering Complexity (design flexibility)	Freq. band	Compactness
[12]	0	High	X band	Low
[13]	0	High	-	Low
[14]	1	High	C band	Mid
[15]	0.3	High	Ku band	High
[16]	0	High	Ku band	High
[17]	0.0075	High	K band	Mid
[18]	0	Low	Ku band	Low
[19]	0	High	Ku band	High
[20]	0	Low	X band	Mid
[21]	0	High	W band	Mid
[22]	0	High	X band	Mid
[23]	0.22	High	Ka band	High
[24]	0	High	Ka band	High
[25]	0.3	High	V band	High
[26]	1.48	High	X band	Mid
[27]	0.46	High	Ka band	Mid
[28]	1	High	Ka band	Mid
[29]	0	Low	Ku band	Mid
[30]	1.42	High	Ka band	Mid
This work	1.2	Low	Ka band	Mid

band of operation. Relative to the other LWA-based NFF solutions, the structure proposed in this work offers an increased scanning range at *Ka*-band while simultaneously offering a less complicated approach of tapering β as no mechanical modification of the wave guiding structure is required, given that the phase tuning mechanism is transferred to the cheaply fabricated 3-D printed GRIN lens allowing the use of uniform, untapered LWAs as a feed.

IV. CONCLUSION

In this article, a GRIN lens antenna fed by a slitted waveguide was proposed, and the stated goals of simplifying the scanning by taking advantage of the inherent frequency-scanning characteristics of the slitted waveguide were verified by simulation and experiment. The additional goal of simplifying the design of the LWA capable of NFF by separating the feed and phase tuning mechanisms was successfully demonstrated as the proposed structure was shown to be capable of NFF and the focusing spot produced by the prototype was shown to have a displacement along the *z*-direction of about 124 mm. In addition to the optimization of the fabrication of the dielectric fillings to improve the scanning performance of the proposed structure, future work would investigate the possibility of focusing in both the E-plane and H-plane as this work was only concerned with focusing in the H-plane.

ACKNOWLEDGMENT

The authors would like to thank the staff at the Tohoku University production technology department and the Tohoku University innovation plaza and especially K. Okiyama, Y. Imai, and T. Miura for their technical advice in the fabrication of the prototype presented herein.

REFERENCES

[1] A. Mikaelian and A. Prokhorov, "V self-focusing media with variable index of refraction," in *Progress in Optics*, vol. 17. Amsterdam, The Netherlands: Elsevier, 1980, pp. 279–345.

[2] Y. J. Guo, M. Ansari, R. W. Ziolkowski, and N. J. G. Fonseca, "Quasi-optical multi-beam antenna technologies for B5G and 6G mmWave and THz networks: A review," *IEEE Open J. Antennas Propag.*, vol. 2, pp. 807–830, 2021.

[3] F. Fan, M. Cai, J. Zhang, Z. Yan, and J. Wu, "Wideband low-profile Luneburg lens based on a glide-symmetric metasurface," *IEEE Access*, vol. 8, pp. 85698–85705, 2020.

[4] O. Zetterstrom, N. J. G. Fonseca, and O. Quevedo-Teruel, "Compact half-Luneburg lens antenna based on a glide-symmetric dielectric structure," *IEEE Antennas Wireless Propag. Lett.*, vol. 21, pp. 2283–2287, 2022.

[5] A. Buffi, P. Nepa, and G. Manara, "Design criteria for near-field-focused planar arrays," *IEEE Antennas Propag. Mag.*, vol. 54, no. 1, pp. 40–50, Feb. 2012.

[6] P. Nepa and A. Buffi, "Near-field-focused microwave antennas: Near-field shaping and implementation," *IEEE Antennas Propag. Mag.*, vol. 59, no. 3, pp. 42–53, Jun. 2017.

[7] J. Bor, B. Fuchs, O. Lafond, and M. Himdi, "Flat foam-based Mikaelian lens antenna for millimeter wave applications," in *Proc. 11th Eur. Radar Conf.*, Rome, Italy, Oct. 2014, pp. 337–340.

[8] J. W. Yang, W. Y. Lai, H. C. Chou, and M. N. M. Kehn, "Compact Mikaelian lens synthesized by metasurfaces," *IEEE Antennas Wireless Propag. Lett.*, vol. 17, pp. 397–400, 2018.

[9] E. I. Semernya and S. P. Skobelev, "Analysis of wave focusing by axisymmetric Mikaelian lenses," *IEEE Antennas Wireless Propag. Lett.*, vol. 20, pp. 269–273, 2021.

[10] W. Shao and Q. Chen, "2-D beam-steerable generalized Mikaelian lens with unique flat-shape characteristic," *IEEE Antennas Wireless Propag. Lett.*, vol. 20, pp. 2033–2037, 2021.

[11] W. Shao and Q. Chen, "Performance analysis of an all-dielectric planar Mikaelian lens antenna for 1-D beam-steering application," *Opt. Exp.*, vol. 29, no. 18, pp. 29202–29214, 2021.

[12] I. Ohtera, "Diverging/focusing of electromagnetic waves by utilizing the curved leakywave structure: Application to broad-beam antenna for radiating within specified wide-angle," *IEEE Trans. Antennas Propag.*, vol. 47, no. 9, pp. 1470–1475, Sep. 1999.

[13] I.-H. Lin, C. Caloz, and T. Itoh, "Near-field focusing by a nonuniform leaky-wave interface," *Microw. Opt. Technol. Lett.*, vol. 44, no. 5, pp. 416–418, Mar. 2005.

[14] J. L. Gomez-Tornero, F. Quesada-Pereira, A. Alvarez-Melcon, G. Goussetis, A. R. Weily, and Y. J. Guo, "Frequency steerable two dimensional focusing using rectilinear leaky-wave lenses," *IEEE Trans. Antennas Propag.*, vol. 59, no. 2, pp. 407–415, Feb. 2011.

[15] A. J. Martínez-Ros, J. L. Gómez-Tornero, F. J. Clemente-Fernández, and J. Monzó-Cabrera, "Microwave near-field focusing properties of width-tapered microstrip leaky-wave antenna," *IEEE Trans. Antennas Propag.*, vol. 61, no. 6, pp. 2981–2990, Jun. 2013.

[16] A. J. Martinez-Ros, J. L. Gómez-Tornero, and G. Goussetis, "Holographic pattern synthesis with modulated substrate integrated waveguide line-source leaky-wave antennas," *IEEE Trans. Antennas Propag.*, vol. 61, no. 7, pp. 3466–3474, Jul. 2013.

[17] T. Okuyama, Y. Monnai, and H. Shinoda, "20-GHz focusing antennas based on corrugated waveguide scattering," *IEEE Antennas Wireless Propag. Lett.*, vol. 12, pp. 1284–1286, 2013.

[18] J. L. Gómez-Tornero, A. J. Martínez-Ros, and J. Monzó-Cabrera, "Demonstration of simple electronic near-field beamforming using multitone microwave signals with a leaky-wave focused applicator," *IEEE Antennas Wireless Propag. Lett.*, vol. 14, pp. 143–146, 2015.

[19] A. J. Martinez-Ros, J. L. Gómez-Tornero, V. Losada, F. Mesa, and F. Medina, "Non-uniform sinusoidally modulated half-mode leaky-wave lines for near-field focusing pattern synthesis," *IEEE Trans. Antennas Propag.*, vol. 63, no. 3, pp. 1022–1031, Mar. 2015.

[20] S. Clauzier, S. Avrillon, L. Le Coq, M. Himdi, F. Colombel, and E. Rochefort, "Slotted waveguide antenna with a near-field focused beam in one plane," *IET Microw., Antennas Propag.*, vol. 9, no. 7, pp. 634–639, May 2015.

[21] R. W. McKinney, Y. Monnai, R. Mendis, and D. Mittleman, "Focused terahertz waves generated by a phase velocity gradient in a parallel-plate waveguide," *Opt. Exp.*, vol. 23, no. 21, p. 27947, 2015.

[22] A. H. Panaretos and D. H. Werner, "Leaky wave lenses for spoof plasmon collimation," *Opt. Exp.*, vol. 24, no. 13, pp. 14654–14671, 2016.

[23] Y. F. Wu, Y. J. Cheng, and Z. X. Huang, "Ka-band near-field-focused 2-D steering antenna array with a focused Rotman lens," *IEEE Trans. Antennas Propag.*, vol. 66, no. 10, pp. 5204–5213, Oct. 2018.

[24] Y. F. Wu and Y. J. Cheng, "Two-dimensional near-field focusing folded reversely fed leaky-wave antenna array with high radiation efficiency," *IEEE Trans. Antennas Propag.*, vol. 67, no. 7, pp. 4560–4569, Jul. 2019.

[25] G.-B. Wu, K. F. Chan, and C. H. Chan, "Holographic amplitude-modulated (AM) leaky-wave antennas for near-field and far-field applications," 2022, *arXiv:2205.09506*.

[26] S. E. Bankov, E. V. Frolova, and V. I. Kalinichev, "Simulation and experimental study of a linear bifocal antenna array," *J. Commun. Technol. Electron.*, vol. 68, no. 1, pp. 40–50, Jan. 2023.

[27] Y. F. Wu and Y. J. Cheng, "Proactive conformal antenna array for near-field beam focusing and steering based on curved substrate integrated waveguide," *IEEE Trans. Antennas Propag.*, vol. 67, no. 4, pp. 2354–2363, Apr. 2019.

[28] T. Hashimoto, H. Sato, and Q. Chen, "Near-field leaky-wave focusing antenna with inhomogeneous rectangular waveguide," *IEICE Commun. Exp.*, vol. 9, no. 6, pp. 218–223, Jun. 2020.

[29] K. K. Mutai, H. Sato, and Q. Chen, "Near-field leaky-wave focusing antenna with tapered dielectric constant distribution," *IEEE Antennas Wireless Propag. Lett.*, vol. 22, pp. 1209–1213, 2023.

[30] K. K. Mutai and Q. Chen, "Frequency scanning leaky-wave array antenna with extended scanning range for millimeter wave imaging," *IEEE Antennas Wireless Propag. Lett.*, vol. 22, no. 8, pp. 1977–1981, Aug. 2023.

[31] I. A. Eshrah, A. A. Kishk, A. B. Yakovlev, and A. W. Glisson, "Rectangular waveguide with dielectric-filled corrugations supporting backward waves," *IEEE Trans. Microw. Theory Techn.*, vol. 53, no. 11, pp. 3298–3304, Nov. 2005.

[32] I. A. Eshrah, A. A. Kishk, A. B. Yakovlev, and A. W. Glisson, "Spectral analysis of left-handed rectangular waveguides with dielectric-filled corrugations," *IEEE Trans. Antennas Propag.*, vol. 53, no. 11, pp. 3673–3683, Nov. 2005.

[33] P. Lampariello and A. A. Oliner, "A novel phased array of printed-circuit leaky-wave line sources," in *Proc. 17th Eur. Microw. Conf.*, Rome, Italy, Oct. 1987.

[34] P. J. B. Clarricoats, P. E. Green, and A. A. Oliner, "Slot-mode propagation in rectangular waveguide," *Electron. Lett.*, vol. 2, no. 8, pp. 307–308, Aug. 1966.

[35] A. Sutinjo, M. Okoniewski, and R. H. Johnston, "Suppression of the slot-mode radiation in a slitted waveguide using periodic slot perturbations," *IEEE Antennas Wireless Propag. Lett.*, vol. 8, pp. 550–553, 2009.

[36] J. L. Gómez-Tornero, J. P. García, and A. Álvarez-Melcón, "Efficient full-wave analysis method of leaky-wave modes in periodically loaded dielectric waveguides with application to backward-to-forward frequency-scannable antennas and metamaterials," *Int. J. Numer. Model., Electron. Netw., Devices Fields*, vol. 19, no. 2, pp. 173–193, Mar. 2006.

[37] K. Nishizawa, "Principle and application on gradient index optical imaging," *Rev. Laser Eng.*, vol. 8, no. 5, pp. 748–758, 1980.

[38] C. Gomez-Reino, M. V. Perez, and C. Bao, *Gradient-Index Optics: Fundamentals and Applications*. New York, NY, USA: Springer, 2002.

[39] W. Shao, H. Sato, X. Li, K. K. Mutai, and Q. Chen, "Perforated extensible 3-D hyperbolic secant lens antenna for directive antenna applications using additive manufacturing," *Opt. Exp.*, vol. 29, no. 12, pp. 18932–18949, 2021.

[40] S. Zhang, R. K. Arya, S. Pandey, Y. Vardaxoglou, W. Whittow, and R. Mittra, "3D-printed planar graded index lenses," *IET Microw., Antennas Propag.*, vol. 10, no. 13, pp. 1411–1419, 2016.

[41] M. Poveda-García, J. L. Gómez-Tornero, and D. Cañete-Rebenaque, "Study of the efficiency of half-width substrate integrated waveguide leaky-wave antennas in FR4," in *Proc. 2nd URSI Atlantic Radio Sci. Meeting (AT-RASC)*, Gran Canaria, Spain, May 2018, pp. 1–4.

Kevin Kipruto Mutai (Graduate Student Member, IEEE) received the B.E. degrees from the Jomo Kenyatta University of Agriculture and Technology (JKUAT), Nairobi, Kenya, in 2017 and 2018, and the M.E. degree from Tohoku University, Sendai, Japan, in 2022, where he is currently pursuing the Ph. D. degree in communications engineering.

His current research interests include leaky wave antennas, active/passive millimeter wave imaging, lens antennas, and electronically reconfigurable antennas.

Mr. Mutai received the Student Presentation Award at the 2020 International Conference on Emerging Technologies on Communications (ICETC2020), the Best Paper Award IEEE Sendai Section in 2022, the IEEE AP-S Japan Student Award in 2023, and was a winner of the 2023 IEEE AP-S Doctoral Fellowship Award.

Qiang Chen (Senior Member, IEEE) received the B.E. degree from Xidian University, Xi'an, China, in 1986, and the M.E. and D.E. degrees from Tohoku University, Sendai, Japan, in 1991 and 1994, respectively.

He is currently a Chair Professor with the Electromagnetic Engineering Laboratory, Department of Communications Engineering, Faculty of Engineering, Tohoku University. His primary research interests include antennas, microwave and millimeter wave, electromagnetics measurement, and computational electromagnetics.

Dr. Chen is a fellow of the Institute of Electronics, Information and Communication Engineers (IEICE). He received the Best Paper Award and Zen-Ichi Kiyasu Award from IEICE, in 2009. He served as the Chair for the IEICE Technical Committee on Photonics-Applied Electromagnetics Measurement, from 2012 to 2014, the Chair for the IEICE Technical Committee on Wireless Power Transfer, from 2016 to 2018, and the Chair for the IEEE Antennas and Propagation Society Tokyo Chapter, from 2017 to 2018. He is currently the Chair of the IEICE Technical Committee on Antennas and Propagation.